Pharm Res (2012) 29:1165–1179
DOI 10.1007/s11095-012-0711-y

EXPERT REVIEW

Magnetic Nanoparticles in Magnetic Resonance Imaging and Diagnostics

Christine Rümenapp • Bernhard Gleich • Axel Haase

Received: 22 September 2011 / Accepted: 15 February 2012 / Published online: 6 March 2012

ABSTRACT Magnetic nanoparticles are useful as contrast agents for magnetic resonance imaging (MRI). Paramagnetic contrast agents have been used for a long time, but more recently superparamagnetic iron oxide nanoparticles (SPIOs) have been discovered to influence MRI contrast as well. In contrast to paramagnetic contrast agents, SPIOs can be functionalized and size-tailored in order to adapt to various kinds of soft tissues. Although both types of contrast agents have a inducible magnetization, their mechanisms of influence on spin-spin and spin-lattice relaxation of protons are different. A special emphasis on the basic magnetism of nanoparticles and their structures as well as on the principle of nuclear magnetic resonance is made. Examples of different contrast-enhanced magnetic resonance images are given. The potential use of magnetic nanoparticles as diagnostic tracers is explored. Additionally, SPIOs can be used in diagnostic magnetic resonance, since the spin relaxation time of water protons differs, whether magnetic nanoparticles are bound to a target or not.

KEY WORDS contrast agent · diagnostic magnetic resonance · magnetic nanoparticles · magnetic resonance imaging · spin relaxation

ABBREVIATIONS

DMR	diagnostic magnetic resonance
DOTA	1,4,7,10-tetraazacyclododecane-1,4,7, 10-tetraacetic acid
DPDP	di-pyridoxyl- di-phosphate
DTPA	diethylene-triamine –pentaacetic acid
HER2	human epidermal growth factor receptor 2
MNP	magnetic nanoparticle
MPI	magnetic particle imaging
MRI	magnetic resonance imaging
PEG	poly-ethylene-glycol
PEI	poly-ethylen-imine
PET	positron emission tomography
SPIO	superparamagnetic iron oxide
VEGF	vascular endothelial growth factor

Christine Rümenapp and Bernhard Gleich contributed equally.

C. Rümenapp · B. Gleich · A. Haase (✉)
Zentralinstitut für Medizintechnik (IMETUM)
Technische Universität München
Boltzmannstr. 11, 85748 Garching, Germany
e-mail: axel.haase@tum.de

INTRODUCTION

Nanoscience and nanotechnology have tremendously influenced research in the fields of biology and medicine over the last few decades.

Applications of engineered nanoparticles related to these fields include targeted drug (1–4) and gene delivery (5,6) as well as agents to enhance the diagnostic possibilities of magnetic resonance imaging (7,8) or the development of new imaging methods (9).

Nanoparticles possess unique properties such as a high surface to volume ratio, their quantum properties (10) and their ability to carry other compounds due to their small size. These characteristics make them attractive for many medical applications.

Next to non-magnetic nanoparticles like liposomes, polymeric micelles, dendrimers and quantum dots, magnetic nanoparticles form an interesting and useful group of nanoparticles. The natural abundance of MNPs in biological systems is very high. All migratory birds, fishes and other animals use magnetic nanoparticles in their geomagnetic navigational aids (11). Ferritin, the most common iron storage protein can contain up to 3000 ferric ions in a paramagnetic

oxyhydroxide core (12). This protein is present in almost every cell of plants, animals and humans. The human brain, for example, contains over 108 magnetite (Fe_3O_4) and maghemite (Fe_2O_3) nanoparticles per gram tissue (13).

Switchable magnetic properties of superparamagnetic nanoparticles make these materials useful for magnetic drug targeting, cell tracking, hyperthermia and medical imaging. Based on their inducible magnetization, SPIO and agents bound to SPIO can be guided to a defined location in an external magnetic gradient field (14,15) or heated up in an external applied oscillating field (16). Thus, SPIOs are attractive for many applications ranging from separation techniques (17), magnetic transfection of cells (18) to contrast enhancing agents for MRI (19–23).

Magnetic resonance imaging on its own has already an outstanding soft tissue contrast. The ongoing development of magnetic nanoparticles as contrast agents further enhances image contrast . New magnetic contrast agents can be size-tailored to accumulate in specific organs (24,25) or their surface can be functionalized to target cells (e.g. tumour cells) specifically (26). Hence, the contrast of MRI is significantly enhanced and diseases can be potentially detected at an earlier stage.

In this article we focus on the basic principles of the magnetism of magnetic nanoparticles as well as on the principles of nuclear magnetic resonance to explain the impact of magnetic nanoparticles on MRI. Based on nuclear magnetic resonance (NMR), we show that magnetic nanoparticles can be used as a diagnostic tool to detect the binding of SPIO with cells and pathogens.

BASIC PRINCIPLES

Magnetic nanoparticles for medical and biological applications can be divided into paramagnetic, ferromagnetic and superparamagnetic particles. The impact of superpara- and ferromagnetic particles on magnetic resonance imaging or diagnostic magnetic resonance is almost equal. The composition of paramagnetic particles is completely diverging from the composition of superpara- and ferromagnetic particles. Superpara- and ferromagnetic particles are composed of a magnetic core and a surface coating (Fig. 1a). Paramagnetic particles are mainly chelates of paramagnetic ions with no explicit core and surface coating (Fig. 1b). Thus, their influence on MRI contrast is rather different from superpara- and ferromagnetic particles.

Additionally to their conventional composition, a new generation of magnetic nanoparticles has been invented more recently. These new particles combine different imaging modalities such as PET and MRI (Fig. 1c). For this purpose SPIOs are combined with PET tracers, ^{64}Cu and ^{18}F for example. With the integration of two imaging modalities molecular information can be visualized together with anatomic details to assist for better medical diagnostics (27).

Magnetism of Magnetic Nanoparticles (MNP)

The material of the core as well as the core's size and shape of a superpara- and ferromagnetic particle mainly define its magnetic properties.

The type of core material defines whether the particle is para- or ferromagnetic at the body's temperature of 310 K. In general, magnetism depends strongly on the temperature. If the temperature is higher than the material specific Curie temperature, ferromagnetism and thus superparamagnetism disappears and the material shows paramagnetic behaviour. The commonly used Gadolinium (Gd^{3+}) based contrast agents are paramagnetic in medical and biological applications.

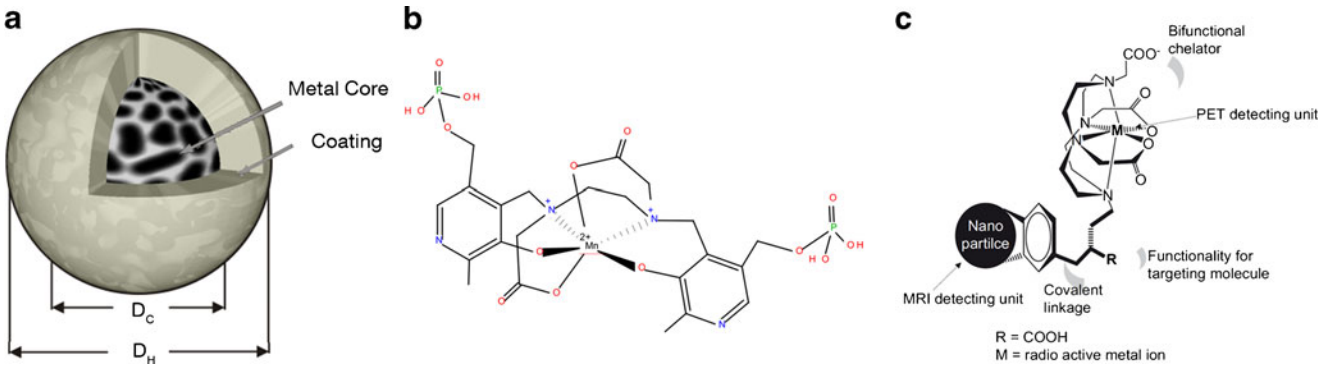

Fig. 1 Overview for the structure of different magnetic particles; (**a**) a simple structure of a magnetic particle with a metal core and a surface coating without any further functionalization (D_C = metal core diameter, D_H = hydrodynamic diameter); (**b**) the structure of a manganese containing contrast agent; the manganese ion is chelated by Dipyridoxal Diphosphate (DPDP). (**c**) a proposed structure of a contrast agent with dual imaging modalities. Next to the magnetic nanoparticle for MRI this structure also contains a radioactive metal ion, M, for PET imaging. (**c**) reprinted with permission from (67).

Paramagnetism

Each atom of a paramagnetic material behaves as individual, non-interacting and randomly orientated molecular magnet with the magnetic dipole moment $\boldsymbol{\mu}_A$. In absence of an external magnetic field the dipoles of a paramagnetic particle are oriented randomly. When an external magnetic field is applied to paramagnetic particles, the molecular magnets start to align with the direction of the external magnetic field. When the magnetic field strength is increased, more and more molecular magnets align with the external field until all molecular magnets are aligned. Complete alignment of the particles with the external field is defined as magnetic saturation. Magnetic saturation in paramagnetic particles can only occur at very low temperatures or at very high magnetic field strengths. Paramagnetic gadolinium chloride for example starts to saturate at approximately 50 T (28). Once the external magnetic field is removed all molecular magnets will instantaneously orientate in a random manner due to thermal fluctuations. Hence, no net magnetization or remanence occurs in paramagnetic particles.

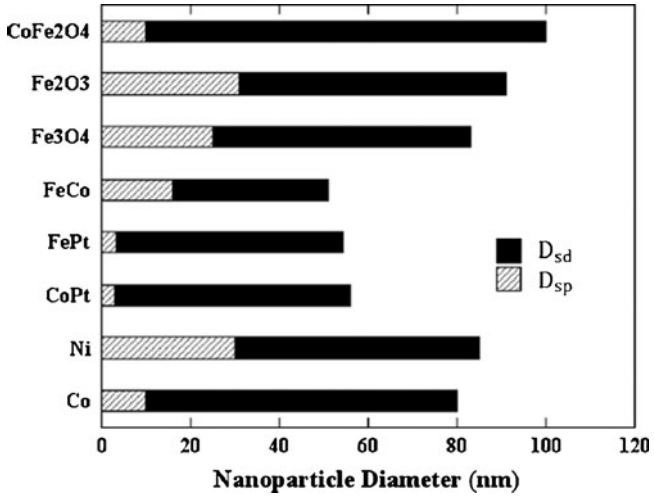

Fig. 2 At a given temperature nanomaterials show a distinctly different behaviour for different sizes. The critical sizes for the observation of superparamagnetism and single-domain behaviour, D_{sp} and D_{sd}, respectively, in a variety of common ferromagnetic fine particles are shown. For core diameters $D_C < D_{sp}$, they exhibit superparamagnetism; for $D_c > D_{sd}$, they split into multiple domains to minimize their overall energy and between $D_{sp} < D_C > D_{sd}$, they are ferromagnetic and single domain. A measurement time of 100 s is assumed in all cases. Reprinted with permission from (37).

Ferromagnetism

Ferromagnetism and cognate magnetism (ferrimagnetism, antiferromagnetism) are characterized by a strong exchange interaction energy, which leads to a regular orientation of the magnetic moments. One ferromagnetic particle is organized in Weiss domains, each separated by a Bloch or a Néel wall (29,30). All of the magnetic dipole moments within each Weiss domain are orientated in the same direction. As long as no external magnetic field is applied, there is no necessity that magnetic moments in different Weiss domains are oriented in the same direction. In the presence of an external magnetic field the domain walls will reorganize and the total magnetic moment, as well as the magnetization M of the ferromagnetic particle, start to align with the external field. After removing the external magnetic field, the magnetization of the ferromagnetic particle can be partially or even fully retained, the particle shows a magnetic remanence and can act as a permanent magnet.

The number of Weiss domains depends strongly on the size of the particle. If the size of the ferromagnetic core D_c is smaller than a critical size D_{sd}, the multiple domain state will be abandoned for the benefit of an energetic more favourable single domain state (Fig. 2). These single domain particles consist of only one Weiss domain, so that all of the internal dipole moments point in the same direction. The magnetic moment of the ferromagnetic single domain particle with volume V and the saturation magnetization M_s is in the range of $V \cdot M_s$. In ferromagnetic single domain particles, magnetization can only be changed by relaxation of the bulk (Brownian relaxation) and the magnetization vector (Néel relaxation) and not due to reorganization of the domain walls (31). Magnetic saturation occurs at small external fields compared to paramagnetic particles. Saturation is achieved, for example, at 1–2.5 T for massive steel and at 0.15–0.25 T for iron oxide nanoparticles (32–35).

Superparamagnetism

If the size of a ferromagnetic single domain particle is further decreased, so that D_c is smaller than a second critical size D_{sp}, superparamagnetism occurs (Fig. 2). In particles smaller than the critical size D_{sp}, thermal fluctuations outcompete the dipole-dipole interactions and cause the magnetization to flip randomly in absence of an external magnetic field (36). Thus, the energy barrier, which separates the ferromagnetic single domain state from the superparamagnetic state, is proportional to the volume of the particle, to the anisotropy constant and to the observation time (37). Furthermore, superparamagnetic particles have, exactly like paramagnetic particles, no net magnetization if no external field is applied. However, the needed external field strength to saturate superparamagnetic particles is comparable to the field strength for ferromagnetic particles (32–35). The critical sizes D_{sd} for ferromagnetic single domain particles and D_{sp} for superparamagnetic particles of different materials are shown in Fig. 2 (37). Particles with sizes larger than D_{sd} consist of multiple Weiss domains.

The influence of the core's shape on the magnetism of the particle will only be addressed briefly. The shape of the ferromagnetic or superparamagnetic core affects the homogeneity of the magnetization. A homogeneous magnetization can only be achieved if the shape is ellipsoidal. Distortions from the ideal shape can lead to destabilization of the single-domain state of the particle (38).

Synthesis and Surface Coating

The bare metal core of magnetic nanoparticles must meet several stability requirements to avoid agglomeration and to obtain stable colloidal suspensions (5,39,40). Magnetic dipole-dipole interactions and van der Waals attractive forces mainly affect this stability. Minor aspects are the stability against settling in the gravitational field and the stability in a magnetic field gradient, which can be achieved by reducing the size and which goes hand in hand with stabilization against magnetic interaction.

To minimize magnetic dipole-dipole interaction, the dipole-dipole contact energy must be smaller than the thermal energy k_BT. For ferromagnetic particles, the dipole-dipole interaction energy depends on the particle's volume. Hence, the size of the particle must be reduced. As long as the dipole-dipole contact energy is much smaller than the thermal energy, the influence on the colloidal stability of magnetic interaction can be neglected (35). Accordingly, for particles based on Fe_3O_4 this is the case for a core diameter smaller than approximately 8 nm (35).

Van der Waals forces arise spontaneously between particles because of fluctuating electric dipole-dipole forces, which are always present on the nanometer scale. Compared to magnetic dipole-dipole interaction van der Waals forces are much larger. The magnitude of interaction decreases with the power of six with the distance for van der Waals interaction and with the power of three with the distance for magnetic interaction. Therefore, stabilization against van der Waals forces is only possible by increasing the distance between the metal cores of single particles and, more effectively, by strong steric repulsion of an applied surface coating.

Furthermore, corrosive effects on bare metal nanoparticles are more present due to their high surface to volume ratio, which makes them more chemical reactive (5).

Besides the preservation of physical stability there are several requirements on magnetic nanoparticles in biological and medical applications. First, toxicity must be avoided. Second, depending on their application it is desired to increase or decrease their circulation time in the cardiovascular system. An increase in circulation time of the nanoparticles allows the detection of structural abnormalities in the cardiovascular system. Since tumours and inflammatory as well as infectious sites show rapid neovasculature, nanoparticles can easily permeate into the surrounding tissue and accumulate (19,41). Contrary, rapid elimination from the body is required to minimize the exposure of the body to the agent as well as interferences with other imaging modalities, e.g. CT (42). Third, their specificity to defined targets (e.g. tumour tissue, specific organs, cells, proteins) needs to be improved.

Gadolinium based paramagnetic agents are obtained by complexation of the Gd^{3+} ion with chelates like Diethylene-Triamine –Pentaacetic Acid (DTPA), 1,4,7,10-tetraazacycloDOdecane-1,4,7,10-Tetraacetic Acid (DOTA) and Di-Pyridoxyl- Di-Phosphate (DPDP) (43). Subsequently, these complexes can be entrapped in capsule systems in two ways. One approach is the entrapment in the interior of proteins like apoferritin or other macromolecular conjugates like dextran, dendrimers or polylysine (43,44). With this loose structure, water molecules can still diffuse through the gaps to allow inner sphere relaxation processes. The other approach is the incorporation into a capsule's membrane or linking the gadolinium chelate to a targeting peptide or small molecule. This method implicates drawbacks like decreased stability of the complex (43).

Manganese based paramagnetic nanoparticles can be classified into two categories; first, the small molecule agents and second the macromolecular agents (45). Small molecule agents are, like Gd-chelates, complexes of Mn^{2+} ions with chelates such as DPDP, DTPA or even porphyrin-rings. These complexes can be further modified by incorporation into lipid bilayers. Macromolecular agents are made of manganese oxides such as MnO, MnO_2 and Mn_3O_4. These oxides are formulated into nano- or microparticles. After dissolution in the cells due to proteolytic degradation these particles convert their MR contrast from T_2 contrast agents to T_1 contrast agents (Mn^{2+}) (45). Superparamagnetic iron oxides (SPIO) are often doped with manganese ions for better sensitivity in their function as contrast agents (45).

Among various crystalline polymorphs of iron oxide, maghemite (Fe_2O_3) and magnetite (Fe_3O_4) are the one with the greatest interest in biological and medical applications (39). These superparamagnetic particles are mainly made using a co-precipitation of Fe^{3+} and Fe^{2+} ions (37,46). While large quantities can be made, it is difficult to obtain consistent physical properties (size, shape and dispersity) (46,47). To circumvent these obstacles new approaches have been developed by adding polymers or polyelectrolytes during co-precipitation (46).In contrast, thermal decomposition of a Fe^{3+} chelate solution does not produce large amounts but a tailoring of the core size to 4–20 nm is possible (47,48). Other methods of preparation of SPIOs are sol-gel reactions, hydrothermal methods and flow injection synthesis (43). Pure metals as core material like Fe and Co have the advantage of better magnetic properties and high saturation

magnetization (49,50). However, their oxidative stability is lower and the toxicity is higher compared to iron oxides. To circumvent these obstacles some particles are made of an elemental iron core and an artificial ferrite shell (Fe@M-Fe_2O_4, M=Fe, Mn, Co) combining biocompability and improved hysteresis (51).

Superparamagnetic particles have been coated with Poly-Ethylene-Glycol (PEG), dextran, chitosan, Poly-Ethylen-Imine (PEI), silica (SiO_2), silanes and phospholipids (39,47,52). All of these polymers and polysaccharides can be further modified with different functional groups like, small molecules, peptides, proteins, aptamers, or even antibodies (46,47). A new way of functionalization was introduced which uses bioorthogonal chemistry making it possible to combine one type of particle with various ligands (53).

Biocompatibility

Free Gd^{3+} ions are cytotoxic and are retained in liver, spleen and bone (54). Their chelates behave differently. Their biocompatibility can be further enhanced by shielding them with other dendrimer-like structures (55) . Gadolinium has many advantages as a paramagnetic contrast agent, but recently it has also been associated with nephrogenic systemic fibrosis (NSF) in patients with severe renal disease or in patients after liver transplantation (45).

Manganese is a natural cellular constituent resembling Ca^{2+}, which often acts as a regulatory cofactor for enzymes and receptors (45). However, its toxicity is also known from dust containing manganese in high doses. Besides this, mainly the brain is vulnerable to manganese exposure. Symptoms comparable to characteristics of Parkinson disease are known (45).

The surface coating of SPIOs mainly influences their pharmacokinetics, cellular uptake and ability to cross biological barriers. Macrophages and mainly proliferating cells are able to internalize MNPs when they are smaller than 100 nm (39). In macrophages this happens via receptor-mediated endocytosis while in proliferating cells, e.g. tumour cells, active internalization takes place, where the uptake occurs by fluid phase endocytosis in the G_1 cell cycle phase (56,57). It has also been shown that the uptake seems to depend on the size of the particles. Particles, which are smaller than 50 nm, need to cluster together on the cells surface for endocytosis. One particle alone will not produce enough ATP in the cell, since only one or few receptors will be targeted. Hence the triggering of a signal cascade, so that the cell's membrane will wrap around the particle, will not occur (47,58).

SPIOs are highly captured in the liver (Kupffer cells), the spleen and the lymph nodes (37,39,57,59). Depending on their size, the way of clearance from circulation differs. Small particles (<5 nm) are mainly renally secreted as was shown by Choi *et al.* By using zwitterionic cysteine coated quantum dots the clearance of the nanoparticles from the body depending on their size and surface charge was followed (42). Particles with the size of 10 to 180 nm are taken up by phagocytotic cells such as Kupffer cells in the liver, macrophages but also microglia in the brain. Their primary elimination from the blood circulation occurs in the reticuloendothelial system (60).

However, the incorporation into hemoglobin of erythrocytes has also been reported (61). Nevertheless, it still needs to be elucidated, how cells can handle the overdose of iron oxide, which is present right after the injection of a contrast agent (62).

Besides the size of MNPs, their uptake depends on other factors like their chemical composition, shape, surface structure and charge, aggregation and solubility, but also on the presence of functional groups or other chemicals (63). Nevertheless, it has to be mentioned that, the smaller the particles, the more reactive is their surface leading to a higher concentration of reactive oxygen species and therefore free radicals in the cells. This in turn causes oxidative stress, inflammation and finally damage to proteins, membranes and DNA (56).

Nuclear Magnetic Resonance

Certain atomic nuclei possess a nuclear spin and thus a permanent magnetic dipole moment. The most important example for medical and biological application is the hydrogen nucleus ^1H in water molecules. In a static main magnetic field $\mathbf{B_0}$, the magnetic dipole moments are pointed either in direction of the main field (lower energy state) or in the opposite direction (higher energy state). The two states are populated according to a Boltzmann distribution by the nuclear spins with a higher population in the lower state at body temperature. This difference in occupation numbers of the two energy states leads to the measureable net magnetization $\mathbf{M_0}$ (Fig. 3a).

Both orientations are linked to slightly different energy states; the energy gap is proportional to the magnitude of the main magnetic field B_0. Transitions between the two states can be achieved by applying a time varying magnetic field perpendicular to the main magnetic field $\mathbf{B_0}$. The frequency of this perturbing magnetic field is given by $\omega = \gamma \cdot B_0$, with the gyromagnetic ratio γ. The value of γ varies for different nuclei. For the proton ^1H the gyromagnetic ratio is 42.6 $MHz \cdot T^{-1}$. Hence, for a typical magnetic resonance imaging device with a B_0 field of about 3 T, a radiofrequency of about 127.8 MHz is needed to flip the net magnetization vector of the nuclei out of its initial orientation. Nuclear resonance imaging devices used for small samples are commercially available up to field strengths of more than 20 T, resulting in a radiofrequency of more than 900 MHz.

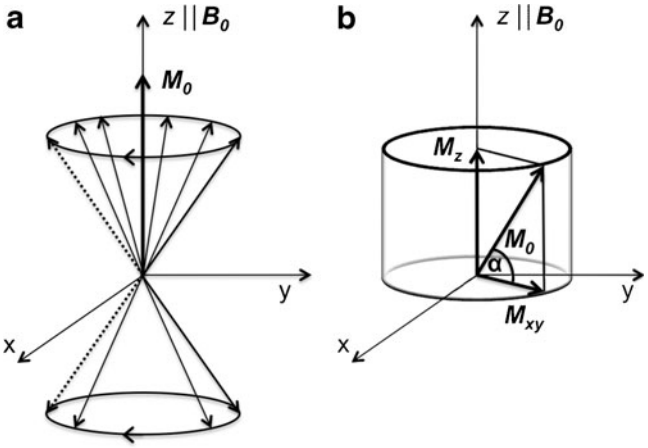

Fig. 3 Illustration of the origin of the nuclear net magnetization $\mathbf{M_0}$ of hydrogen spins in a main magnetic field $\mathbf{B_0}$. (**a**) The Boltzmann distribution of an ensemble of hydrogen nuclei is allowed on two precession cones. In thermal equilibrium the occupation number of the state of lower energy is somewhat higher than that of the state of higher energy leading to the net magnetization $\mathbf{M_0}$. (**b**) Definition of the transversal and longitudinal magnetization; As the net magnetization $\mathbf{M_0}$ precesses in the stationary frame around the z axis, it can be split into two components; the transversal magnetization M_{xy} and the longitudinal magnetization M_z.

If a perturbing magnetic field with the adequate frequency ω and duration τ is irradiated perpendicular to the main magnetic field, the magnetization vector $\mathbf{M_0}$ will be flipped a certain angle (Fig. 3b). The flip angle α is given by $\alpha = \gamma \cdot B_{RF} \cdot \tau$, with the amplitude of the perturbing field B_{RF}. The magnetization parallel to the main magnetic field M_z will be decreased during the irradiation of the perturbing field until its value reaches zero. If the perturbing field is not switched off at this moment, M_Z decreases further and becomes negative (Fig. 3b). Due to the transversal perturbing field the spins are excited to precess in-phase. Thus, the magnetic moments stop annihilating and a rotating magnetization M_{xy} in the x-y plane is the consequence (Fig. 3b).

Immediately after the application of the radiofrequency pulse, a peak signal, which decays very fast (free induction decay, FID), can be detected with a detector coil. The signal arises from the rotating magnetization. The fast signal decay is caused by the relaxation of the transversal magnetization caused by many effects, which are described later.

The original longitudinal magnetization, which was changed after the application of the radiofrequency pulse, will be recovered by the longitudinal or T_1 relaxation.

The longitudinal relaxation causes the system to return to thermal equilibrium due spin-lattice interaction, if only the main magnetic field $\mathbf{B_0}$ acts on the spins (Fig. 3a). It is noteworthy that the $\mathbf{B_0}$ field remains on throughout the experiment. The regrowth of the net longitudinal magnetization is characterized by the T_1 relaxation time, which is given by Eq. 1:

$$M_z(t) = M_{z,0}\left(1 - e^{-\frac{t}{T_1}}\right) \quad (1)$$

with the magnetization $M_{z,0}$ in equilibrium state (64,65). T_1 is defined as the time required after the radio frequency pulse for the magnetization M_z to reach 63% of the original magnetization $M_{z,0}$ (Fig. 4).

Typical samples in magnetic resonance experiments are large compared to single atoms or molecules, each with one or several individual spins. All of these spins experience local differences in the homogeneous main magnetic field $\mathbf{B_0}$ caused by spin-spin interactions. Thus these effects will affect transverse relaxation after the application of a radiofrequency pulse. The transverse relaxation time (T_2) is also called spin-spin relaxation. The precessions of the spins are slightly different among each other in an increasingly dispersed distribution, leading to a signal decay of M_{xy}.

The spins are dephasing after the application of the radio frequency pulse. The decay of the magnetization M_{xy} is given by Eq. 2:

$$M_{xy}(t) = M_{xy,0}\left(e^{\left(-\frac{t}{T_2}\right)}\right) \quad (2)$$

with the initial transversal magnetization $M_{xy,0}$. T_2 is defined as the time duration until 63% of the transversal magnetization is lost (Fig. 4).

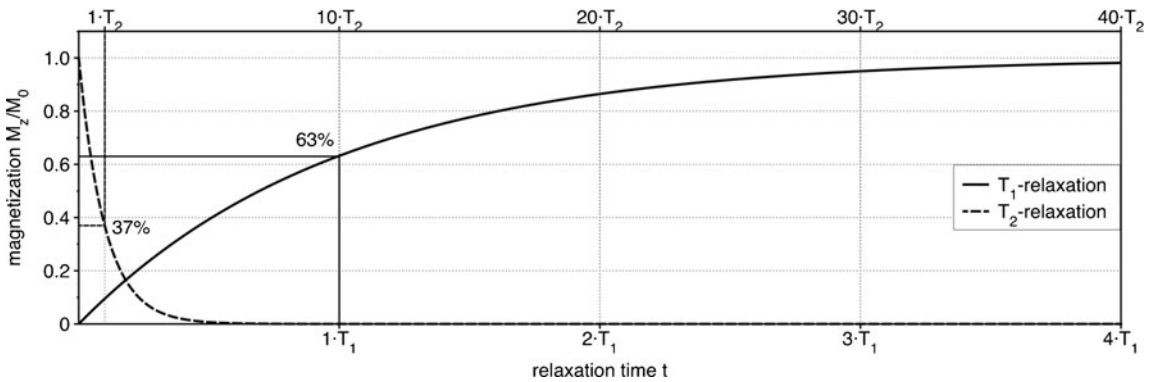

Fig. 4 Relaxation of the longitudinal and the transversal magnetization after the flipping of the net magnetization $\mathbf{M_0}$ with an angle of 90°; M_z relaxes back to the net magnetization $\mathbf{M_0}$. M_{xy} relaxes towards 0.

Both, T_1 and T_2 relaxation processes are executed independently and simultaneously. At the field strengths used in magnetic resonance imaging, the duration of the T_1 relaxation process depends on the magnetic field strength of B_0, whereas the T_2 relaxation process is almost B_0-independent (21). The T_2 relaxation process rather depends the magnetic dipole-dipole interactions, on the diffusion constant of the protons and on the field inhomogeneities. In most cases, the T_2 relaxation time is shorter than the T_1 relaxation time. An imperfect magnetic main field or high magnetic dipole moments of e.g. superparamagnetic nanoparticles can cause magnetic inhomogeneities. Consequently, the observed transverse relaxation time (T_2*) is even shorter than the natural T_2 time caused by spin-spin interactions.

Impact of Magnetic Nanoparticles on Nuclear Magnetic Resonance

Magnetic Dipole Moment

The magnetic moment μ of a magnetic dipole in a given magnetic field B follows a Langevin function, given by Eq. 3 (35):

$$\mu = \mu_{sat} \cdot L(B) \tag{3}$$

with the saturation of the magnetic moment μ_{sat} and the Langevin term given by Eq. 4:

$$L(B) = \coth\left(\frac{\mu_{sat}B}{k_B T}\right) - \frac{k_B T}{\mu_{sat}B} \tag{4}$$

The net magnetization can be estimated using the number of magnetic dipoles inside a nanoparticle when interactions between single dipoles are neglected.

The magnetic field generated by a magnetic dipole moment is given by magnetostatics and is shown in Fig. 2. The influence on the homogeneity of an external main magnetic field and hence indirect the impact on relaxation times are shown in Fig. 5 for both paramagnetic (Fig. 5a and b) and ferromagnetic/superparamagnetic nanoparticles (Fig. 5c and d) with a total magnetization M. The ferromagnetic/superparamagnetic nanoparticle is fully aligned with the external field, whereas the paramagnetic particle is only partially aligned with the external field. Both Fig. 5b and d show the field lines of the corresponding magnetic dipole moment of the magnetic particle and Fig. 5a and c show the distortion of the homogeneity of the external field B_0. It can clearly be seen that the perturbation of the B_0 field is much higher for ferromagnetic/superparamagnetic particles than for paramagnetic particles. The colour scheme indicates the degree of disturbance of the B_0 field. Brighter areas indicate higher disturbances; darker areas indicate weaker perturbation of the external magnetic field. The degree of disturbance was normalized to the corresponding maximum value (Fig. 5).

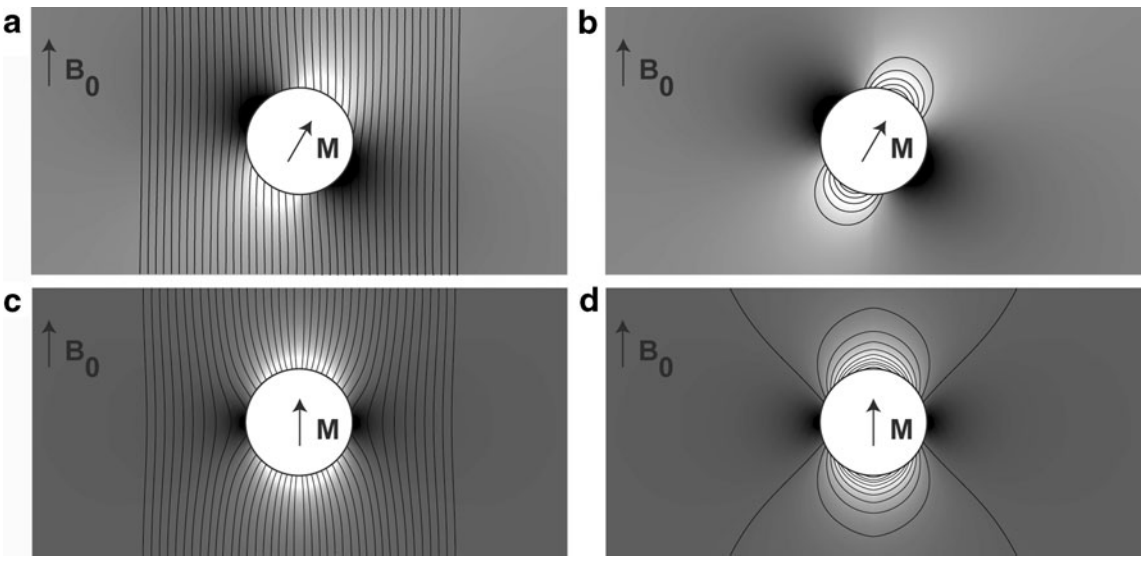

Fig. 5 The figure shows the magnetic field of a superparamagnetic (**c**, **d**) dipole moment of single domain particle and of a paramagnetic (**a**, **b**) particle. Shown are the magnetic field lines (**a**, **c**) and the contour lines of the magnitude of the magnetic field (**b**, **d**). **M** indicates the direction of the magnetization vector and $\mathbf{B_0}$ the external homogenous magnetic field. The lighter shadings denote higher disturbances whereas the darker areas indicate lower disturbances. Take note that the colour scheme is normalized to the corresponding maximum value so that both rows cannot be compared to absolute values.

Paramagnetic Particles—Inner Sphere Relaxation

Gd^{3+} and Mn^{2+} ions are the most frequently used paramagnetic ions for MRI contrast agents (43,66–68). Gd^{3+} has seven and Mn^{2+} has five unpaired electrons, which results in large magnetic moments and in long electronic relaxation times (69,70). The exchange interaction between the electrons of the ions and the neighbouring protons becomes larger than the dipolar interaction between them. Hence, the T_1 relaxation time of the protons will be shortened. To obtain significant changes in proton relaxation and therefore a good contrast, the paramagnetic ion needs to be in close contact to the protons of the surrounding water molecules. Due to this inner sphere relaxation, all paramagnetic contrast agents consist of Gd^{3+} or Mn^{2+} chelates (Fig. 1b) and contain no metal core nor direct surface coating (Fig. 1a). Although paramagnetic complexes generate field inhomogeneities as well (Fig. 5a and b) their influence on T_2 relaxation time of the protons is usually smaller than on T_1 relaxation time.

Superparamagnetic Particles—Outer Sphere Relaxation

The field strength in commonly used MRI scanners is sufficient to saturate the magnetization of superparamagnetic particles. Hence, the orientations of all dipole moments of the particles are aligned with the field. The only modulation of the dipolar interaction between proton spin and the dipole moment of the particle is the diffusion of water protons adjacent to the particles (12,59). This effect is called outer sphere relaxation. Due to the high susceptibility of the superparamagnetic particles large local field inhomogeneities are generated (Fig. 5c and d). This leads to large local field gradients, which accelerate the dephasing of the proton spins. A strong reduction of T_2 relaxation time and a relative small influence on T_1 relaxation time are the consequences (71). Iron oxides are widely used as superparamagnetic contrast agents due to their strong magnetic properties in medical imaging (8,24,43,59).

Relaxivity and Relaxation Rate of Magnetic Particles

Relaxivity (r_1, r_2) measures the ability of any kind of magnetic particles to influence either longitudinal relaxation time T_1 (r_1) or transverse relaxation time T_2 (r_2) or both of the surrounding water proton spins. It is measured *in vitro* and represents the relaxation enhancement of water protons by the contrast agent at a 1 mM concentration (44). Relaxivity of a compound depends mainly on the type of tissue, the material of the particle and the magnitude of the main magnetic field B_0. Usually, relaxivity is given in $mM^{-1}\cdot s^{-1}$. Transverse relaxivity of superparamagnetic nanoparticles can be as high as 148 $mM^{-1}\cdot s^{-1}$ for Feridex, a commercially available MRI contrast agent (67), whereas longitudinal relaxivity is far below 30 $mM^{-1}\cdot s^{-1}$ (59). The longitudinal relaxivity of manganese oxide based paramagnetic agents determined in 1% agarose gel is in the range of 10–20 $mM^{-1}\cdot s^{-1}$ (67). Hence, relaxivity can be used to characterize contrast agents in magnetic resonance imaging for the study of specific tissue areas or simply to achieve a better image quality. In diagnostic magnetic resonance applications, relaxivity is measured to gain information about the linkage between functionalized nanoparticles and biological material. The relaxation rates R_1 and R_2 are quantities, which are derived from the relaxivity for longitudinal (T_1) and transverse (T_2) relaxation. Relaxation rates are the reciprocals of the corresponding relaxation time. In many cases the relation between concentration of the contrast agent, the relaxivity and thus the change in relaxation time is linear (72,73) as follows:

$$R_1 = \frac{1}{T_1} \propto r_1 \times c \tag{5}$$

$$R_2 = \frac{1}{T_2} \propto r_2 \times c \tag{6}$$

The relaxation rates are influenced by the diffusion velocity of protons and hence by the molecule structure. Fat, as an example, has a larger molecule structure than water and thus a slower diffusion velocity than water. This results in a larger relaxation rate and thus in a shorter relaxation time. The introduction of relaxivites and relaxation rates allows the characterization of different agents in regard with their increase of contrast in magnetic resonance imaging.

MEDICAL AND BIOLOGICAL APPLICATIONS

Magnetic Resonance Imaging

In the early seventies of the last century, Lauterbur and Mansfield showed that NMR can be made spatially selective (74,75). If we apply a magnetic field gradient in one of the spatial domains, we measure a NMR signal, having a frequency distribution proportional to this gradient. Magnetic field gradients can be applied in three directions offering three-dimensional spatial information. As a result, NMR shows the spatial distribution of ^1H signals (i.e. water molecules) in an object. In addition, it is possible to create NMR images by applying special NMR pulse sequences having an image contrast according to different relaxation times but also with respect to other physical and chemical parameters, like blood flow, diffusion

constants or even different metabolites. An NMR pulse sequence consists of a defined number of radio frequency pulses in an exactly defined time schedule. These radio frequency pulses can vary in their time duration, their number of repetitions and the pauses between them. The images obtained with NMR pulse sequences show differences depending on their weighting (T_1-weighted or T_2-weighted). Therefore, it is possible to apply NMR pulse sequences, in which tissue with a long T_1 and T_2 relaxation time appears dark in T_1-weighted images and bright in T_2-weighted images. In contrast, tissue with a short T_1 relaxation time and a long T_2 relaxation time, like fat, appears bright in the T_1-weighted images and grey in the T_2-weighted image.

Gadolinium based contrast agents lead to a reduction in T_1 relaxation time and therefore to a positive (brighter) contrast in T_1-weighted images (Fig. 6) (76). Contrast agents based on iron oxides shorten the T_2 relaxation time and thus appear hypointense in T_2-weighted images (Fig. 7a and b) (77).

Besides the development of new contrast agents, research is also carried out to improve the MRI acquisition methods. For the detection of SPIOs spin-echo (SE) pulse sequences and T_2*-weighted gradient echo (GRE) pulse sequences have been traditionally used (24). These are modified now by employing a steady-state acquisition (FIESTA) or even pulse sequences like fluid attenuated inversion-recovery (FLAIR). The FLAIR sequence was until now used for T_1-weighted images and not for T_2-weighted acquisition (48). These new sequences are classified as selective radio frequency pulse methods, dephased methods, and off-resonance methods. In addition, post-processing methods are being developed (48). All these efforts aim for better image contrast and shorter acquisition time.

Cellular and Molecular Imaging

Weissleder *et al.* investigated the visualisation of migrating cells like lymphocytes, monocytes and embryonic stem cells loaded with MNPs via MRI (78). They found that the relaxation rate R_2 increased upon internalisation of the MNPs by the cells compared to MNPs free in solution. As an example, we performed NMR experiments using a NMR spectrometer (Avance 250, Bruker, Karlsruhe, Germany) to determine the T_2 relaxation time of cells loaded with SPIOs. K562 cells were loaded with iron oxide magnetic nanoparticles (size 100 nm) with a silica coating and functionalized with streptavidin (SiMag-Streptavidin, chemicell GmbH, Berlin, Germany). The transverse relaxivity of the particles was calculated as the slope of the curves from R_2 against the iron concentration. Its value out of 4 replicates was 6.068 $mM^{-1}s^{-1}$ (correlation: 0.96558) at 5.8 T. Cells were cultured at 37°C, 10% CO_2 atmosphere with Dulbecco's modified Eagle Medium (Biochrom AG, Berlin, Germany) supplemented with 5% fetal calf serum and penicillin-streptomycin (Biochrom AG, Berlin, Germany). They were loaded over night with 20 pg iron per cell. Suspensions of the particles were given directly into the cell culture medium. The incorporation of the particles was verified by transferring the cells into cell culture dishes and, subsequently, observing the cells' movement in a known magnetic field gradient using an inverted light microscope (Zeiss Axiovert 200, Carl Zeiss Jena GmbH, Jena, Germany) (79). 200 µl of the labelled cell suspension were transferred to 5 mm NMR tubes and each measurement was done in four replicates.

T_2 values were obtained after calibration from 15 data points generated with Carr-Purcell-Meiboom-Gill (CPMG) pulse sequence. Quantitative data is represented as mean ± standard deviation in Table I.

The data in Table I shows that cells loaded with nanoparticles lead to a different signal loss in T_2-weighted MR images compared to particles, which are not incorporated in cells. The same effect was also proofed for ultra-small SPIOs (USPIO). These particles, as well, showed in their intracellular location a more pronounced signal altering effect than being freely in solution (80).

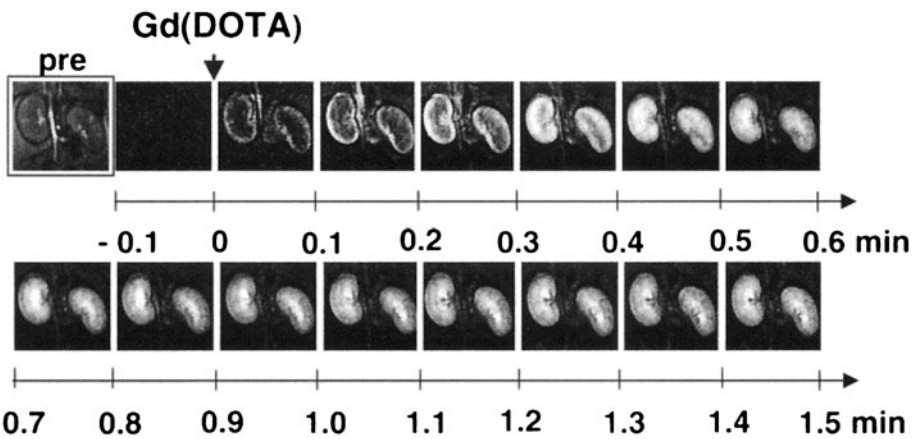

Fig. 6 Time-resolved MRI of Gd (DOTA) passage through the rat kidney; The images presented show the difference images of I(t)-I (pre). I(t) represents the image recorded at time t and I(pre) the image recorded 0.3 min before the administration of Gd(DOTA). High intensity in the images reflect high concentration of Gd(DOTA). The passage of the contrast agent from the renal cortex to the outer medulla and finally to the inner medulla can clearly be seen. Reprinted with permission from (76).

This signal altering effect can be successfully used to track cells *in vivo* using high-resolution MRI. Besides this feature, the particles used were not only magnetic but also fluorescent and additionally had a radiotracer, which made positron emission tomography (PET) possible. After intravenous injection into mice, these cells were visualized by MRI, retrieved from excised tissues using magnetic separation techniques and were still able to differentiate. In stem cell-based therapies this aspect is important for the analysis of site-specific effects on stem cell differentiation. Other stem cells have been loaded as well like mesenchymal stem cells and embryonic stem cells (24). Their migration could be followed in animal models for up to 3 weeks.

As another example, in a MRI study at 11.7 T field strength human mesenchymal stem cells were loaded with superparamagnetic iron oxide particles. The cells were incorporated in hydrogel at different concentrations. The presence of the magnetically labelled stem cells were visualized by distinct hypointense spots in the MR images (Fig. 7c) (81). This effect is also clearly visible for *in vivo* MRI applications.

Taking advantage of the phagocytosis of ultra-small SPIO by macrophages, inflammatory and degenerative diseases can be visualized using MRI (24). After their administration SPIOs are internalized by macrophages, which are attracted to their place of action due to inflammation responses. Hence, focal ischaemic lesions in the cardiovascular system (41), atherosclerosis (26), multiple sclerosis, as well as all kinds of infections can be imaged indirectly by visualizing macrophages loaded with ultra-small SPIO. Additionally, the imaging of transplant rejection and myocarditis can be visualized due to internalization of MNPs by macrophages (19). Since macrophages are accumulated in the lymph nodes, millimetre sized metastases in the lymph nodes can be revealed by MRI before the lymph node enlarges (41). But not just cardiovascular diseases can be monitored using SPIO and MRI, also imaging in the central nervous system can be improved (60).

Molecular imaging is also investigated using Gd-complexes, which are conjugated to enzymes, other proteins or DNA and uptaken by cells via endocytosis (44). Upon internalization the relaxivity of the Gd-complexes changes. With this difference the presence of ligands or other enzymes can be detected.

Also specific biomarkers known from the field of oncology, like HER2 (Human Epidermal growth factor Receptor 2) or VEGF (Vascular Endothelial Growth Factor) can be targeted by the magnetic particles and visualized (48,82). In case of the detection of cardiovascular diseases the Vascular Cell Adhesion Molecule-1 (VCAM-1) has also been monitored (26). Early lesions in atherosclerosis were detected in young mice as well as excised human carotid artery plaques (41). To even detect intracellular markers, like the nuclear marker Ki-67 or the cytoplasmic cytokeratin, and other mediators of cell activation, like p53 or EGFR, this approach was also successfully used on semipermeabilised cells ex vivo (83).

Diagnostic Magnetic Resonance

Another aspect of SPIOs was elucidated over 20 years ago. It was found that the huge pool of ferritin in organs, like liver and spleen, contributes to a signal loss in MRI, which was not explicable with the known relaxation theories (12). It was found that for the same amount of magnetized material, the change of the R_2 value is greater, when fewer

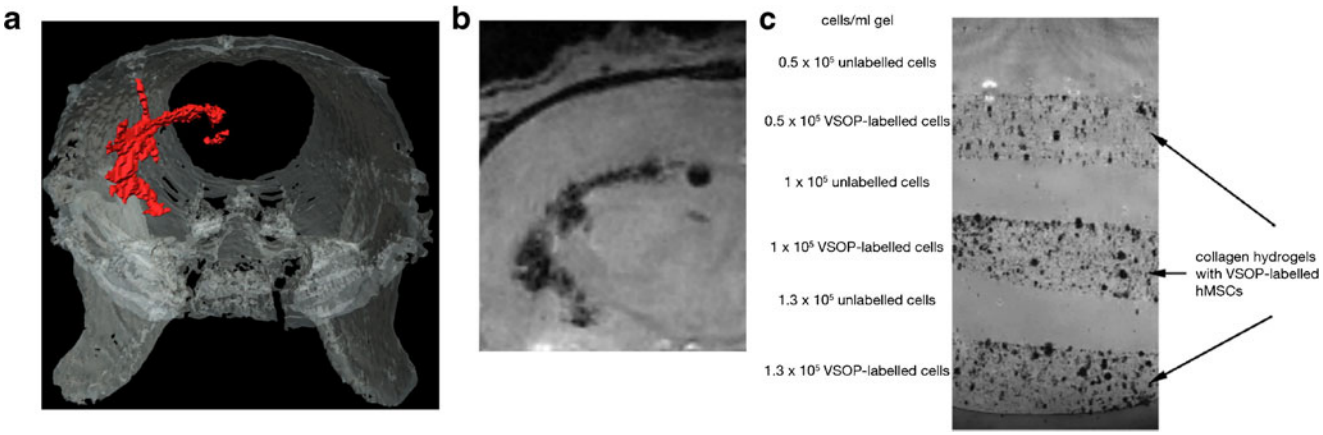

Fig. 7 Examples of MR images using iron oxide based contrast agents: (**a**, **b**) Stem cells labelled with very small superparamagnetic iron oxide particles were transplanted into a rat brain. (**a**) 3D-volume rendering of the stem cells (*red*) in the brain; part of the skull and jaw bones are illustrated for orientation; (**b**) 2D gradient echo MR image through the brain with the cells being observed as dark area. (**a**, **b**) reprinted with permission from (77). (**c**) MR images of human mesenchymal stem cells in collagen type I hydrogels. Magnetically labelled stem cells showed a signal decrease due to iron particles, present as *dark spots*. Control collagen gels with unlabeled cells showed a homogeneous appearance without dark spots. The MRI method was a rapid gradient echo with a nominal spatial resolution of 78 μm and an echo time of 20 ms. (**c**) is reprinted with permission from (81).

Table I T_2 Relaxation Times for Streptavidin Particles in Buffer, K562 Cells and K562 Cells Loaded With Streptavidin Particles (20 pg Fe/cell)

	T_2 in ms
streptavidin particles 100 nm in buffer[a]	17.60 ± 0.81
K562 cells	435.83 ± 113.87
K562 loaded with streptavidin particles 100 nm	268.88 ± 18.53

[a] Particles were measured with the same concentration as it was used to load the cells

but larger particles are present, compared to more but smaller particles. Therefore, the secular contribution to R_2 was introduced in addition. R_1 always decreases towards zero with high external fields applied, whereas R_2 disperses to a non-zero value, which is field-independent. This value, the secular contribution, is usually 20% of its low field limit, but its precise value depends on the relaxation mechanism. This non-dispersive term results from fluctuations of the internal magnetic field caused by MNPs for example parallel to the external static field B_0. These fluctuations cause phase shifts in the Larmor precession of the magnetization of the proton ensemble. If they have a random component, they contribute to R_2. All other contributions to R_1 and R_2 are nonsecular and result from fluctuations of components of the local field within the transverse plane (12).

Muller *et al.* examined the influence on R_2 relaxivity when particles are aggregating (84). For an agglomeration of the MNPs a decrease of 25% in the transverse decay rate was observed over 30 min. If the sample was removed from the magnet and then reinserted, the relaxation rate returned to its initial value to decrease again with time (Fig. 8a). Therefore, the property of SPIOs as contrast agents to shorten the magnetic relaxation of water protons can be improved due to aggregation (Fig. 8b).

When the agglomeration of SPIO cores occurs, the effect on the transverse relaxation of the water protons is enhanced, because of an increase of the secular part of the transverse relaxivity (85).

The effects appearing after the aggregation of the SPIO are two-fold: first, there are those related to the structure of the cluster and to the magnetic field distribution around it (T_2 and T_2*); second, there are those limited to the inner part of the cluster (T_1). In contrast to T_2, clustering of the SPIO does not shorten T_1.

First, the clustering of MNPs is increasing the transverse relaxation time, but second another benefit can be taken out of the induced clustering of MNPs due to static magnetic fields: No static magnetic field is necessary for the detection of concentrations of targets above 1 nM.

To detect small antigen concentrations below 1 nM the number of MNPs in solution also has to be decreased for clustering formation, thus the particles' colliding rate decreases as well. The probability of recognition of antigens by grafted receptors on MNPs is proportional to their colliding rate. To increase this rate, a homogeneous magnetic field (20 mT to 60 mT) can be applied. In this case it is energetically favourable for the particles to self-assemble into chains. Thus, the probability recognition rate between grafted receptors and their ligands is increased. A concentration threshold of antigen as low as 1 pM was detected (86).

A new detection method was developed based on three phenomena: the decrease in R_2 relaxation rate of water protons, when MNPs are clustering, the low detection threshold for protein interactions due to the magnetic

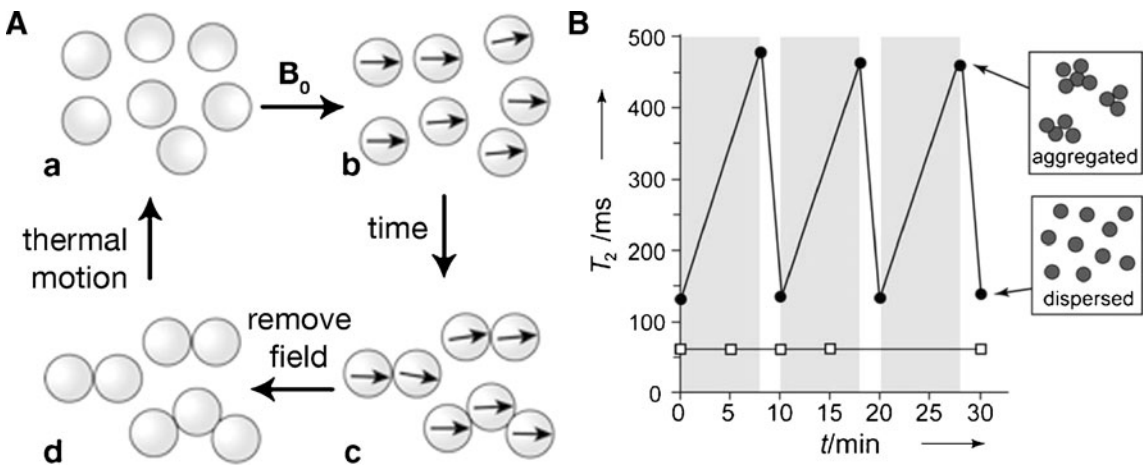

Fig. 8 Principles of diagnostic magnetic resonance; (**A**) When dispersed magnetic particles (**a**) are exposed to an external magnetic, field their magnetic moments will align (**b**). With time, the particles will form aggregates (**c**), which will disperse again due to thermal motion (**a**) and loss of magnetisation (**d**) if the magnetic field is removed. Reprinted with permission from (101). (**B**) Behaviour of magnetic nanoparticles, NP (*white squares*, 30 nm size), and micrometer sized particles, MP (*black dots*, 1000 nm size), in a homogeneous magnetic field (0.47 T). White areas indicate that no field was applied. The T_2 value for MP increased when the field was applied. Reprinted with permission from (90).

induced clustering of MNP, and the independence of T_1 to the clustering of the MNPs (87). In this approach MNPs are called magnetic relaxation switches and are used to detect DNA and proteins down to the femtomolar level even in unpurified samples. By using this method not only DNA and proteins, but bacteria, viruses or even specific cells like tumour cells can be detected (87–92).

We used the biotin-streptavidin system to further investigate this approach. Magnetic nanoparticles with coupled streptavidin with a diameter of 100 nm were used (SiMag-Streptavidin, chemicell GmbH, Berlin, Germany). T_2 values were obtained using the same setup as for the cellular measurements mentioned before. T_2 was measured with the particles diluted 1:200 in phosphate buffered saline (PBS) containing 0.1 mg/ml BSA and 0.1% BSA, after incubation with 16 μM biotin, and with biotin bound to agarose beads and unconjugated agarose beads (both obtained from Vector Laboratories, Burlingame, USA). 200 μl of the suspensions were transferred to 5 mm NMR tubes each and the concentration of the particles was always kept the same. Each measurement was done in 4 replicates and quantitative data are represented as mean ± standard deviation in Table II.

As one can see in Table II, T_2 relaxation times differ, whether biotin is bound to the streptavidin particles or not. To vary the size of the target in this experiment, biotin was one time unbound and the other time bound to agarose beads. We could not see a difference in the measured T_2 relaxation time. However, others have shown that besides the size of MNPs also the size and valency of the target is crucial for the detection limit of the method (91). They investigated two sizes of particles with variable target analytes (the valencies and the sizes were different) under the use of a single molecular recognition system. For small MNPs (30 nm) the sensitivity improved using a bigger target and a higher valency of the target, whereas bigger MNPs (1 μm) were more sensitive to small and low valency targets. Small MNPs show a decrease in T_2 upon aggregation, whereas bigger MNPs show an increase in T_2.

Next to the fact that high concentrations of the analyte will saturate the receptors and prevent further crosslinking and reduce the sensitivity, the aspect of the valency of the particles has also to be carefully considered. If the agglomerates get to big, this could also lead to their precipitation (89).

To take advantage of the phenomenon of the magnetic relaxation switches, particles with an improved T_2 relaxivity and diagnostic magnetic resonance devices (DMR) are being developed.

The first device for point of care diagnostics using DMR was developed in the group of R. Weissleder (93). Consisting of permanent magnets with B_0 up to 0.5 T (21.3 MHz) and a μNMR chip containing a 2×4 planar micro coil array on a glass substrate, 8 multiplexed measurements of 5–10 μl samples were possible. Its detection limit was 1 pM, similar to the detection method of Baudry *et al*, who used optical measurements for the determination of the target protein concentration (86). They further improved the device by reducing the sample volume to 1 μl, so that the SNR would be higher (94). Furthermore, they built in an automated feedback system to track and compensate for temperature drift, and used a mobile device to facilitate the control of the system and to share the data over wireless networks (95). The detection limit for cells was reduced to 2 cells / 1 μl. To reduce the risk of false positive results they decreased the incubation time from 30 min to 5 min. With this it is possible to obtain results in less than 60 min. The first application on human tumour samples was very promising. An accuracy of 96% compared to standard of care procedures was achieved (96).

CONLCUSIONS

Superparamagnetic iron oxide particles are fairly easy to make and provide the basis for various applications. Due to their magnetic behaviour they proof to be excellent contrast agents and efforts are taken to improve their target specificity. With their help it is possible to detect diseases like inflammatory diseases (cardiovascular diseases, multiple sclerosis, atherosclerosis or infections) or cancer in an earlier stage or to monitor their development. Nevertheless, their synthesis and their functionalization are still under investigation.

The design objectives for the next generation of MR contrast agents will also include their prolonging intravascular

Table II T2 Relaxation Times Measured for Different Biotin-Streptavidin Setups Displayed in ms

Biotin bound to agarose beads	Biotin bound to agarose beads with streptavidin particles	Streptavidin particles in buffer
206.45 ± 37.74	17.65 ± 0.83	24.29 ± 8.65
agarose beads	agarose beads incubated with streptavidin particles	
172.87 ± 55.78	23.83 ± 2.09	
16 μM Biotin	16 μM Biotin incubated with streptavidin particles	
73.4 ± 11.79	17.07 ± 1.75	

retention, improved tissue targeting, as well as the combination with different imaging modalities. To combine these different imaging methods such as MRI and PET, new particles made up of SPIOs conjugated with radioactive tracers are developed (Fig. 1) (97). But also the combination of magnetic nanoparticles with fluorescent dyes or both, fluorescent dyes and radioactive tracers are under investigation (98).

Due to their magnetic properties SPIOs can also be used for targeted drug delivery systems by loading them with the necessary drug and guiding them to the point of interest using external magnetic fields (99). Selective targeting due to their clearance in spleen and liver has also been reported (100). The SPIOs are loaded with a drug for chemotherapy and MRI visualizes their presence in the liver.

With all their advantages and benefits the possible toxicity of magnetic nanoparticles should not be neglected and each particle type needs to be scrutinized for its biocompability.

However, not just the particle itself is under investigation but also the MRI acquisition methods. They are modified to differentiate between the signal loss due to air bubbles or due to SPIOs or even new methods are developed to improve the image contrasts provided by SPIOs (48).

Besides their application in MRI, a new imaging method using magnetic particles has been developed. Magnetic particle imaging (MPI) relies on the nonlinear magnetization response of superparamagnetic nanoparticles to generate a tomographic image (9). This new imaging method is characterized by both high spatial resolution and high sensitivity. Here, the combination of MRI and MPI in one instrument is also envisioned.

The improvement of detection limits of SPIOs is necessary to pave the way for newly designed SPIOs into clinical application. SPIOs have gained interest due to their ability to give diagnostic information and being able to deliver therapeutics at the same time. Nevertheless, the reproducible synthesis of SPIOs and a better understanding of the influence of the polymeric coating of a SPIO on its magnetic properties are goals, which still have to be fulfilled. This issue should be kept in mind for the development of the next generation of SPIOs for MRI.

ACKNOWLEDGMENTS & DISCLOSURES

We thank J. Hintermair and A. Heidsieck, Zentralinstitut für Medizintechnik (IMETUM), Technische Universität München, Germany for performing cell culture and computer simulation and S. Glaser, Chemistry Department, Technische Universität München, Germany, for providing the NMR spectrometers.

This work was partly supported by a grant of the Deutsche Forschungsgesellschaft (DFG, grant no. GL 661/1-1) within the Research Unit 917 "Nanoparticle-based targeting of gene- and cell-based therapies".

REFERENCES

1. Alexiou C, Jurgons R, Schmid RJ, Hilpert A, Bergemann C, Parak FG, *et al. In vitro* and *in vivo* investigations of targeted chemotherapy with magnetic nanoparticles. J Magn Magn Mater. 2005;293:389–93.
2. Widder KJ, Senyei AE. Magnetic microspheres: A vehicle for selective targeting of drugs. Pharmacol Ther. 1983;20(3):377–95.
3. Luebbe AS, Alexiou C, Bergemann C. Clinical applications of magnetic drug targeting. J Surg Res. 2001;95(2):200–6.
4. Häfeli U. Magnetically modulated therapeutic systems. Int J Pharm. 2004;277(1–2):19–24.
5. McBain S, Yiu H, Dobson J. Magnetic nanoparticles for gene and drug delivery. Int J Nanomedicine. 2008;3(2):169–80.
6. Scherer F, Anton M, Schillinger U, Henke J, Bergemann C, Krüger A, *et al.* Magnetofection: enhancing and targeting gene delivery by magnetic force *in vitro* and *in vivo*. Gene Therapy. 2002;9(2):102–9.
7. Kirsch J. Basic principles of magnetic resonance contrast agents. Top Magn Reson Imag. 1991;3(2):1–18.
8. Weissleder R, Elizondo G, Wittenberg J, Lee A, Josephson L, Brady T. Ultrasmall superparamagnetic iron oxide: an intravenous contrast agent for assessing lymph nodes with MR imaging. Radiology. 1990;175(2):494–8.
9. Gleich B, Weizenecker J. Tomographic imaging using the nonlinear response of magnetic particles. Nature. 2005;435 (7046):1214–7.
10. Roduner E. Size matters: why nanomaterials are different. Chem Soc Rev. 2006;35(7):583–92.
11. Rancourt DG. Magnetism of Earth, planetary and environmental nanomaterials. In: Jillian FB, Alexandria N, editors. Nanoparticles and the enviroment: Mineralogical Society of America and The Geochemical Society. 2001;44:217–92.
12. Gillis P, Koenig Seymour H. Transverse relaxation of solvent protons induced by magnetized spheres: Application to ferritin, erythrocytes, and magnetite. Magn Reson Med. 1987;5(4):323–45.
13. Kirschvink J, Kobayashi-Kirschvink A, Woodford B. Magnetite biomineralization in the human brain. Proc Natl Acad Sci U S A. 1992;89(16):7683–7.
14. Alexiou C, Diehl D, Henninger P, Iro H, Rockelein R, Schmidt W, *et al.* A high field gradient magnet for magnetic drug targeting. IEEE Trans Appl Supercond. 2006;16(2):1527–30.
15. Plank C. Nanomagnetosols: magnetism opens up new perspectives for targeted aerosol delivery to the lung. Trends Biotechnol. 2008;26(2):59–63.
16. Jordan A, Scholz R, Wust P, Fähling H, Felix R. Magnetic fluid hyperthermia (MFH): Cancer treatment with AC magnetic field induced excitation of biocompatible superparamagnetic nanoparticles. J Magn Magn Mater. 1999;201(1–3):413–9.
17. Rembaum A, Yen R, Kempner D, Ugelstad J. Cell labeling and magnetic separation by means of immunoreagents based on polyacrolein microspheres. J Immunol Methods. 1982;52 (3):341–51.
18. Plank C, Schillinger U, Scherer F, Bergemann C, Rémy J-S, Krötz F, *et al.* The magnetofection method: using magnetic force to enhance gene delivery. Biol Chem. 2003;384(5):737–47.

19. Sosnovik DE, Nahrendorf M, Weissleder R. Magnetic nanoparticles for MR imaging: agents, techniques and cardiovascular applications. Basic Res Cardiol. 2008;103(2):122–30.
20. Schlorf T, Meincke M, Kossel E, Gluer C, Jansen O, Mentlein R. Biological properties of iron oxide nanoparticles for cellular and molecular magnetic resonance imaging. Int J Mol Sci. 2010;12 (1):12–23.
21. Stanisz G, Odrobina E, Pun J, Escaravage M, Graham S, Bronskill M, *et al.* T1, T2 relaxation and magnetization transfer in tissue at 3T. Magn Reson Med. 2005;54(3):507–12.
22. Tysiak E, Asbach P, Aktas O, Waiczies H, Smyth M, Schnorr J, *et al.* Beyond blood brain barrier breakdown - *in vivo* detection of occult neuroinflammatory foci by magnetic nanoparticles in high field MRI. J Neuroinflammation. 2009;6:20.
23. Hofmann-Amtenbrink M, Hofmann H, Montet X. Superparamagnetic nanoparticles - a tool for early diagnostics. Swiss Med Wkly. 2010;140:w13081.
24. Corot C, Robert P, Idée J, Port M. Recent advances in iron oxide nanocrystal technology for medical imaging. Adv Drug Deliv Rev. 2006;58(14):1471–504.
25. Chouly C, Pouliquen D, Lucet I, Jeune J, Jallet P. Development of superparamagnetic nanoparticles for MRI: effect of particle size, charge and surface nature on biodistribution. J Microencapsul. 1996;13(3):245–55.
26. McCarthy J, Weissleder R. Multifunctional magnetic nanoparticles for targeted imaging and therapy. Adv Drug Deliv Rev. 2008;60(11):1241–51.
27. Nahrendorf M, Sosnovik DE, Weissleder R. MR-optical imaging of cardiovascular molecular targets. Basic Res Cardiol. 2008 Mar;103(2):87–94.
28. Zborowski A, Chalmers JJ. Magnetic cell seperation. In: van der Vliet P, Pillai S, editors: Laboratory Techniques in Biochemistry and Molecular Biology. Elsevier; 2003;32.
29. Kittel C. Physical theory of ferromagnetic domains. Rev Mod Phys. 1949;21(4):541–83.
30. Frei E, Shtrikman S, Treves D. Critical size and nucleation field of ideal ferromagnetic particles. Phys Rev. 1957;106(3):446–55.
31. Kötitz R, Fannin P, Trahms L. Time domain study of Brownian and Néel relaxation in ferrofluids. J Magn Magn Mater. 1995;149(1–2):42–6.
32. Kim T, Reis L, Rajan K, Shima M. Magnetic behavior of iron oxide nanoparticle biomolecule assembly. J Magn Magn Mater. 2005;295:132–8.
33. Eberbeck D, Trahms L. Experimental investigation of dipolar interaction in suspensions of magnetic nanoparticles. J Magn Magn Mater. 2011;323:1228–32.
34. Ferguson R, Minard Kevin R, Krishnan Kannan M. Optimization of nanoparticle core size for magnetic particle imaging. J Magn Magn Mater. 2009;321(10):1548–51.
35. Rosensweig RE. Ferrodynamics: The behavior and dynamics of magnetic fluids receive a coherent, comprehensive treatment in this high-level study, encompassing electromagnetism and fields, magnetocaloric energy conversion, ferrohydrodynamic instabilities, and related subjects. Geared toward graduate students and researchers in physics, engineering, and applied mathematics. Preface. Appendixes. References. Indexes. Dover Publications. 1997.
36. Brown WF. Thermal fluctuations of a single-domain particle. Phys Rev. 1963;130(5):1677–86.
37. Krishnan K. Biomedical nanomagnetics: a spin through possibilities in imaging, diagnostics, and therapy. IEEE Trans Magn. 2010;46 (7):2523–58.
38. Cowburn R. Property variation with shape in magnetic nanoelements. J Phys D: Appl Phys. 2000;33(1):1.
39. Chomoucka J, Drbohlavova J, Huska D, Adam V, Kizek R, Hubalek J. Magnetic nanoparticles and targeted drug delivering. Pharmacol Res. 2010;62(2):144–9.
40. Lalatonne Y, Richardi J, Pileni M. Van der Waals *versus* dipolar forces controlling mesoscopic organizations of magnetic nanocrystals. Nat Mater. 2004;3(2):121–5.
41. Sun C, Lee JS, Zhang M. Magnetic nanoparticles in MR imaging and drug delivery. Adv Drug Deliv Rev. 2008;60(11):1252–65.
42. Choi HS, Liu W, Misra P, Tanaka E, Zimmer JP, Itty Ipe B, *et al.* Renal clearance of quantum dots. Nat Biotechnol. 2007;25(10):1165–70.
43. Ai H. Layer-by-layer capsules for magnetic resonance imaging and drug delivery. Adv Drug Deliv Rev. 2011;63(9):772–88.
44. Aime S, Cabella C, Colombatto S, Geninatti Crich S, Gianolio E, Maggioni F. Insights into the use of paramagnetic Gd(III) complexes in MR-molecular imaging investigations. J Magn Reson Imaging. 2002;16(4):394–406.
45. Pan D, Caruthers SD, Senpan A, Schmieder AH, Wickline SA, Lanza GM. Revisiting an old friend: manganese-based MRI contrast agents. Wiley Interdiscip Rev Nanomed Nanobiotechnol. 2010.
46. Lodhia J, Mandarano G, Ferris N, Eu P, Cowell S. Development and use of iron oxide nanoparticles (Part 1): synthesis of iron oxide nanoparticles for MRI. Biomed Imag Interv J. 2010;6(2):e12.
47. Veiseh O, Gunn J, Zhang M. Design and fabrication of magnetic nanoparticles for targeted drug delivery and imaging. Adv Drug Deliv Rev. 2010;62(3):284–304.
48. Stephen Zachary R, Kievit Forrest M, Zhang M. Magnetite nanoparticles for medical MR imaging. Mater Today. 2011;14 (7–8):330–8.
49. Arias J, Lopez-Viota M, Ruiz M, Lopez-Viota J, Delgado A. Development of carbonyl iron/ethylcellulose core/shell nanoparticles for biomedical applications. Int J Pharm. 2007;339(1–2):237–45.
50. Pouponneau P, Leroux J, Martel S. Magnetic nanoparticles encapsulated into biodegradable microparticles steered with an upgraded magnetic resonance imaging system for tumor chemoembolization. Biomaterials. 2009;30(31):6327–32.
51. Yoon T, Lee H, Shao H, Weissleder R. Highly magnetic core-shell nanoparticles with a unique magnetization mechanism. Angew Chem Int Ed Engl. 2011;50(20):4663–6.
52. Drbohlavova J, Hrdy R, Adam V, Kizek R, Schneeweiss O, Hubalek J. Preparation and properties of various magnetic nanoparticles. Sensors. 2009;9(4):2352–62.
53. Haun J, Devaraj N, Hilderbrand S, Lee H, Weissleder R. Bioorthogonal chemistry amplifies nanoparticle binding and enhances the sensitivity of cell detection. Nat Nanotechnol. 2010;5(9):660–5.
54. Wiegers CB, Welch MJ, Sharp TL, Brown JJ, Perman WH, Sun Y, *et al.* Evaluation of two new gadolinium chelates as contrast agents for MRI. Magnet Res Imaging. 1992;10(6):903–11.
55. Lei X, Jockusch S, Turro N, Tomalia D, Ottaviani M. EPR characterization of gadolinium(III)-containing-PAMAM-dendrimers in the absence and in the presence of paramagnetic probes. J Colloid Interface Sci. 2008;322(2):457–64.
56. Mahmoudi M, Azadmanesh K, Shokrgozar M, Journeay W, Laurent S. Effect of nanoparticles on the cell life cycle. Chem Rev. 2011;111(5):3407–32.
57. Moore A, Weissleder R, Bogdanov A. Uptake of dextran-coated monocrystalline iron oxides in tumor cells and macrophages. J Magn Reson Imaging. 1997;7(6):1140–5.
58. Chithrani B, Chan W. Elucidating the mechanism of cellular uptake and removal of protein-coated gold nanoparticles of different sizes and shapes. Nano Lett. 2007;7(6):1542–50.
59. Gossuin Y, Gillis P, Hocq A, Voung QL, Roch A. Magnetic Resonance Relaxation properties of superparamagnetic particles. Wileys Interdiscipl Rev: Nanomed Nanobiotech. 2009;1:299–310.
60. Weinstein JS, Varallyay CG, Dosa E, Gahramanov S, Hamilton B, Rooney WD, *et al.* Superparamagnetic iron oxide nanoparticles: diagnostic magnetic resonance imaging and potential therapeutic applications in neurooncology and central nervous system inflammatory pathologies, a review. J Cereb Blood Flow Metab. 2010;30(1):15–35.

61. Weissleder R, Stark D, Engelstad B, Bacon B, Compton C, White D, *et al.* Superparamagnetic iron oxide: pharmacokinetics and toxicity. Am J Roentgenol. 1989;152(1):167–73.
62. Lévy M, Lagarde F, Maraloiu V, Blanchin M, Gendron F, Wilhelm C, *et al.* Degradability of superparamagnetic nanoparticles in a model of intracellular environment: follow-up of magnetic, structural and chemical properties. Nanotechnology. 2010;21 (39):395103.
63. Thorek D, Tsourkas A. Size, charge and concentration dependent uptake of iron oxide particles by non-phagocytic cells. Biomaterials. 2008;29(26):3583–90.
64. Bloch F. Nuclear induction. Phys Rev. 1946;70(7–8):460–74.
65. Purcell E, Torrey H, Pound R. Resonance absorption by nuclear magnetic moments in a solid. Phys Rev. 1946;69(1–2):37–8.
66. Caravan P, Ellison JJ, McMurry TJ, Lauffer RB. Gadolinium(III) chelates as MRI contrast agents: structure, dynamics, and applications. Chem Rev. 1999;99(9):2293–352.
67. Patel D, Kell A, Simard B, Xiang B, Lin H, Tian G. The cell labeling efficacy, cytotoxicity and relaxivity of copper-activated MRI/PET imaging contrast agents. Biomaterials. 2011;32 (4):1167–76.
68. Kurki T, Komu M. Spin-lattice relaxation and magnetization transfer in intracranial tumors *in vivo*: effects of Gd-DTPA on relaxation parameters. Magnet Res Imaging. 1995;13(3):379–85.
69. Bloembergen N. Proton relaxation times in paramagnetic solutions. J Chem Phys. 1957;27(2):572–3.
70. Bloembergen N, Morgan LO. Proton relaxation times in paramagnetic solutions effects of electron spin relaxation. J Chem Phys. 1961;34(3):842–50.
71. Pankhurst Q, Connolly J, Jones S, Dobson J. Applications of magnetic nanoparticles in biomedicine. J Phys D: Appl Phys. 2003;36(13):167.
72. Gossuin Y, Roch A, Muller Robert N, Gillis P. An evaluation of the contributions of diffusion and exchange in relaxation enhancement by MRI contrast agents. J Magnet Res. 2002;158(1–2):36–42.
73. Reiser MF, Semmler W, Hricak H. Magnetic resonance tomography. Springer: Berlin, Heidelberg; 2008.
74. Lauterbur PC. Image formation by induced local interactions - examples employing nuclear magnetic-resonance. Nature. 1973;242(5394):190–1.
75. Mansfield P, Grannell PK. NMR 'diffraction' in solids? J Phys C: Solid State Phys. 1973;6(22):L422.
76. Baumann D, Rudin M. Quantitative assessment of rat kidney function by measuring the clearance of the contrast agent Gd (DOTA) using dynamic MRI. Magnet Res Imaging. 2000;18 (5):587–95.
77. Stroh A, Faber C, Neuberger T, Lorenz P, Sieland K, Jakob P, *et al. In vivo* detection limits of magnetically labeled embryonic stem cells in the rat brain using high-field (17.6 T) magnetic resonance imaging. NeuroImage. 2005;24(3):635–45.
78. Weissleder R, Cheng H-C, Bogdanova A, Bogdanov A. Magnetically labeled cells can be detected by MR imaging. J Magn Reson Imaging. 1997;7(1):258–63.
79. Haefeli U, Lobedann M, Steingroewer J, Moore L, Riffle J. Optical method for measurement of magnetophoretic mobility of individual magnetic microspheres in defined magnetic field. J Magn Magn Mater. 2005;293:224–39.
80. Fleige G, Seeberger F, Laux D, Kresse M, Taupitz M, Pilgrimm H, *et al. In vitro* characterization of two different ultrasmall iron oxide particles for magnetic resonance cell tracking. Invest Radiol. 2002;37(9):482–8.
81. Heymer A, Haddad D, Weber M, Gbureck U, Jakob P, Eulert J, *et al.* Iron oxide labelling of human mesenchymal stem cells in collagen hydrogels for articular cartilage repair. Biomaterials. 2008;29(10):1473–83.
82. Gore J, Manning H, Quarles C, Waddell K, Yankeelov T. Magnetic resonance in the era of molecular imaging of cancer. Magn Reson Imaging. 2011;29(5):587–600.
83. Haun J, Devaraj N, Marinelli B, Lee H, Weissleder R. Probing intracellular biomarkers and mediators of cell activation using nanosensors and bioorthogonal chemistry. ACS Nano. 2011;5 (4):3204–13.
84. Muller RN, Gillis P, Moiny F, Roch A. Transverse relaxivity of particulate MRI contrast media: from theories to experiments. Magn Reson Med. 1991;22(2):178–82.
85. Roch A, Gossuin Y, Muller Robert N, Gillis P. Superparamagnetic colloid suspensions: water magnetic relaxation and clustering. J Magnet Magnet Mater. 2005;293:532–9.
86. Baudry J, Rouzeau C, Goubault C, Robic C, Cohen-Tannoudji L, Koenig A, *et al.* Acceleration of the recognition rate between grafted ligands and receptors with magnetic forces. Proc Natl Acad Sci U S A. 2006;103(44):16076–8.
87. Perez J, Josephson L, Weissleder R. Use of magnetic nanoparticles as nanosensors to probe for molecular interactions. ChemBioChem. 2004;5(3):261–4.
88. Aurich K, Nagel S, Glöckl G, Weitschies W. Determination of the magneto-optical relaxation of magnetic nanoparticles as a homogeneous immunoassay. Anal Chem. 2007;79(2):580–6.
89. Kim G, Josephson L, Langer R, Cima M. Magnetic relaxation switch detection of human chorionic gonadotrophin. Bioconjug Chem. 2007;18(6):2024–8.
90. Koh I, Hong R, Weissleder R, Josephson L. Sensitive NMR sensors detect antibodies to influenza. Angew Chem Int Ed Engl. 2008;47(22):4119–21.
91. Koh I, Hong R, Weissleder R, Josephson L. Nanoparticle-target interactions parallel antibody-protein interactions. Anal Chem. 2009;81(9):3618–22.
92. Quillard T, Croce K, Jaffer F, Weissleder R, Libby P. Molecular imaging of macrophage protease activity in cardiovascular inflammation *in vivo*. Thromb Haemost. 2011;105 (5):828–36.
93. Lee H, Sun E, Ham D, Weissleder R. Chip-NMR biosensor for detection and molecular analysis of cells. Nat Med. 2008;14 (8):869–74.
94. Lee H, Yoon T, Weissleder R. Ultrasensitive detection of bacteria using core-shell nanoparticles and an NMR-filter system. Angew Chem Int Ed Engl. 2009;48(31):5657–60.
95. Issadore D, Min C, Liong M, Chung J, Weissleder R, Lee H. Miniature magnetic resonance system for point-of-care diagnostics. Lab Chip. 2011;11(13):2282–7.
96. Haun J, Castro C, Wang R, Peterson V, Marinelli B, Lee H, *et al.* Micro-NMR for rapid molecular analysis of human tumor samples. Sci Transl Med. 2011;3(71):71ra16.
97. Choi J, Park J, Nah H, Woo S, Oh J, Kim K, *et al.* A hybrid nanoparticle probe for dual-modality positron emission tomography and magnetic resonance imaging. Angew Chem Int Ed Engl. 2008;47(33):6259–62.
98. Nahrendorf M, Keliher E, Marinelli B, Waterman P, Feruglio P, Fexon L, *et al.* Hybrid PET-optical imaging using targeted probes. Proc Natl Acad Sci U S A. 2010;107(17):7910–5.
99. Alexiou C, Tietze R, Schreiber E, Jurgons R, Richter H, Trahms L, *et al.* Cancer therapy with drug loaded magnetic nanoparticles - magnetic drug targeting. J Magn Magn Mater. 2011;323:1404–7.
100. Maeng J, Lee D, Jung K, Bae Y, Park I, Jeong S, *et al.* Multifunctional doxorubicin loaded superparamagnetic iron oxide nanoparticles for chemotherapy and magnetic resonance imaging in liver cancer. Biomaterials. 2010;31(18):4995–5006.
101. Hong R, Cima M, Weissleder R, Josephson L. Magnetic microparticle aggregation for viscosity determination by MR. Magn Reson Med. 2008;59(3):515–20.